


# Echolocation-inspired memristive behavioral decision circuit

Yueqi Song(宋钥淇), Xiaozhou He(何晓舟), Xianying Xu(徐宪莹), Yinghong Cao(曹颖鸿), Santo Banerjee, Suo Gao(高锁), and Jun Mou(牟俊)

**Citation:**Chin. Phys. B, 2026, 35 (**6**): 060701. DOI: 10.1088/1674-1056/ae2d3e
http://cpb.iphy.ac.cn; http://iopscience.iop.org/cpb

**What follows is a list of articles you may be interested in**

---

## FPGA based hardware platform for trapped-ion-based multi-level quantum systems

Ming-Dong Zhu(朱明东), Lin Yan(闫林), Xi Qin(秦熙),Wen-Zhe Zhang(张闻哲), Yiheng Lin(林毅恒), and Jiangfeng Du(杜江峰)

Chin. Phys. B, 2023, 32 (**9**): 090702. DOI: 10.1088/1674-1056/accb48

## A spintronic memristive circuit on the optimized RBF-MLP neural network

Yuan Ge(葛源), Jie Li(李杰), Wenwu Jiang(蒋文武), Lidan Wang(王丽丹), and Shukai Duan(段书凯)

Chin. Phys. B, 2022, 31 (**11**): 110702. DOI: 10.1088/1674-1056/ac6b1d

## A terahertz on-chip InP-based power combiner designed using coupled-grounded coplanar waveguide lines

Huali Zhu(朱华利), Yong Zhang(张勇), Kun Qu(屈坤), Haomiao Wei(魏浩淼), Yukun Li(黎雨坤), Yuehang Xu(徐跃杭), and Ruimin Xu(徐锐敏)

Chin. Phys. B, 2021, 30 (**12**): 120701. DOI: 10.1088/1674-1056/ac05af

## A high performance fast-Fourier-transform spectrum analyzer for measuring spin noise spectrums

Yu Tong(仝煜), Lin Wang(王淋), Wen-Zhe Zhang(张闻哲), Ming-Dong Zhu(朱明东), Xi Qin(秦熙), Min Jiang(江敏), Xing Rong(荣星), Jiangfeng Du(杜江峰)

Chin. Phys. B, 2020, 29 (**9**): 090704. DOI: 10.1088/1674-1056/ab9c04

## Microfluidic temperature sensor based on temperature-dependent dielectric property of liquid

Qi Liu(刘琦), Yu-Feng Yu(俞钰峰), Wen-Sheng Zhao(赵文生), Hui Li(李慧)

Chin. Phys. B, 2020, 29 (**1**): 010701. DOI: 10.1088/1674-1056/ab593c

---

**SPECIAL TOPIC — Biophysical circuits: Modeling & applications in neuroscience**

# Echolocation-inspired memristive behavioral decision circuit

Yueqi Song(宋钥淇)[1], Xiaozhou He(何晓舟)[2,†], Xianying Xu(徐宪莹)[1], Yinghong Cao(曹颖鸿)[1], Santo Banerjee[3], Suo Gao(高锁)[1], and Jun Mou(牟俊)[1,‡]

[1] *School of Information Science and Engineering, Dalian Polytechnic University, Dalian* 116034, *China*
[2] *School of Network Information Center, Dalian Medical University, Dalian* 116044, *China*
[3] *Department of Mathematical Sciences, Giuseppe Luigi Lagrange, Politecnico di Torino, Corso Duca degli Abruzzi* 24, *Torino, Italy*

(Received 19 November 2025; revised manuscript received 10 December 2025; accepted manuscript online 16 December 2025)

Memristive circuits have been widely employed to emulate various neural behavioral mechanisms. However, most existing works remain focused on isolated learning processes and have not yet established behavioral systems capable of adapting to changing stimuli, transitioning across perceptual states, and preserving behavioral continuity. To address these limitations, an echolocation-inspired memristive behavioral decision circuit is proposed in this work. The framework is organized into four functional modules — Stimulus, Action, Decision-making, and Memory — which operate cooperatively to enable behavioral generation that transitions from stimulus-driven responses to experience-driven execution across different conditions. Under strong stimulus conditions, behavior is directly elicited by external sensory input; under weak stimulus conditions, decision reliability is maintained through internal regulation; and under no-stimulus conditions, behavioral continuity is preserved through experience-based bias and memory replay. PSPICE simulations verify that the circuit maintains stable decision outputs and functional continuity across all conditions, demonstrating its effectiveness for biologically inspired and adaptive decision-making in neuromorphic systems.

**Keywords:** echolocation, volatile memristor, memristive circuit, decision-making module

**PACS:** 07.05.Mh, 07.50.–e

**DOI:** 10.1088/1674-1056/ae2d3e **CSTR:** 32038.14.CPB.ae2d3e

## 1. Introduction

In nature, biological organisms are able to regulate their behavior and make decisions in complex environments through perception, learning, and memory.[1–3] For example, bats rely on echolocation to navigate and hunt in complete darkness, where sensory perception and motor control are achieved through a dynamical cycle of stimulus, response, and memory.[4–7] It is worth noting that such behavior is not driven solely by instantaneous sensory input, but is instead produced through the coupling of external stimuli, internal state estimation, and previously acquired experience. When external sensory signals are weakened or completely absent, behavioral control is gradually shifted from stimulus-driven computation to strategies based on internal prediction and memory bias, thereby ensuring behavioral continuity.

Inspired by such biological capabilities, it is increasingly recognized that artificial intelligence (AI) systems also require mechanisms for real-time stimulus response,[8,9] internal state regulation, and experience-based memory utilization. However, conventional digital computing architectures and fixed-structure neural networks typically rely on global clocks and discrete update mechanisms, making it difficult to support multi-timescale learning, continuous state evolution, and behavioral persistence within a unified framework.[10–12] In recent years, memristors have attracted increasing attention due to their plasticity,[13–16] history-dependent dynamics, and synapse-like behavior, and they are regarded as promising candidates for modeling biological learning and behavioral mechanisms.[17–19] Their conductance states can evolve dynamically in response to input and remain stored after stimulus removal, thereby providing a unified physical substrate for real-time sensing, internal regulation, and long-term memory.[20–22]

Since Chua[23] introduced the memristor as the fourth fundamental circuit element in 1971, it has been recognized for non-volatility, tunable resistance, and history dependence. Owing to this property, memristors inherently exhibit non-volatile storage, analog resistance modulation, and dependence on historical excitation patterns.[24,25] A specific subclass known as threshold memristors is particularly well suited for neuromorphic applications. These devices introduce switching thresholds and nonlinear state transitions, allowing them to retain memory, adjust synaptic weights, and express activity-dependent plasticity similar to biological synapses.[26] Consequently, threshold-type devices have become key building blocks in brain-inspired circuit architectures and are

†Corresponding author. E-mail: hexiaozhou@dmu.edu.cn
‡Corresponding author. E-mail: junmou@dlpu.edu.cn

© 2026 Chinese Physical Society and IOP Publishing Ltd. All rights, including for text and data mining, AI training, and similar technologies, are reserved.

widely used to model synaptic dynamics under different neuronal states.[27–29] Threshold memristors, in particular, provide memory retention, nonlinear switching, and adjustable synaptic strength, enabling dynamical reproduction of synaptic plasticity.[30,31] They have been widely employed in brain-inspired circuits, such as associative memory,[32–34] episodic neural networks,[35–37] and emotional memory circuits,[38–40] underscoring their essential role in neuromorphic design. Nevertheless, most existing memristive circuits focus on single synaptic modulation or learning functions and lack investigations into integrated perception-decision-memory behavioral processes.[41,42] Moreover, dynamical behavioral switching under strong, weak, and no-stimulus conditions has rarely been reported.

In this work, an echolocation-inspired memristive behavioral decision circuit is presented, consisting of four modules — stimulus, action, decision, and memory. Volatile and non-volatile memristors are employed to realize short-term synaptic plasticity and long-term memory, respectively. The circuit can switch its behavioral mode according to stimulus intensity. PSPICE simulation results demonstrate stable outputs and continuous functional transitions under different stimulus conditions, providing a new approach for biologically inspired behavioral decision modeling.

The remainder of this paper is organized as follows. Section 2 introduces the employed memristor models together with detailed parameter configurations. Section 3 presents the behavioral modes under different stimulus conditions. Section 4 describes the overall circuit architecture and the implementation of each functional module. Section 5 reports the simulation results. Finally, Section 6 concludes this work and looks forward to subsequent research directions.

## 2. Memristor model

### 2.1. Volatile memristive model

A volatile memristor (VM) is a device whose memristance temporarily changes in response to external stimuli and naturally returns to its original state once the stimulus is removed. It does not retain long-term memory but reacts quickly to dynamical inputs, making it ideal for mimicking short-term synaptic plasticity and transient "forgetting" processes observed in biological systems. Additionally, the VM can be reset by applying a voltage, allowing the circuit to start from a consistent initial state for each experimental trial. The model[6] is as follows:

$$\begin{cases} i = (1-x)\alpha[1-\mathrm{e}^{-\beta v}] + xy\sinh(\delta v), \\ \dot{x} = \lambda[\mathrm{e}^{\eta v} - \mathrm{e}^{-\eta v}]f(x) - \frac{x-\varepsilon}{\tau}, \\ \dot{y} = \sigma[\mathrm{e}^{\eta v} - \mathrm{e}^{-\eta v}]f(x), \\ \dot{z} = \theta[\mathrm{e}^{\eta v} - \mathrm{e}^{-\eta v}], \\ f(x) = \frac{(\mathrm{sign}(v)+1)(\mathrm{sign}(1-x)+1)+(\mathrm{sign}(-v)+1)(\mathrm{sign}(x)+1)}{4}, \end{cases} \tag{1}$$

where $v$ and $i$ represent the applied voltage and the corresponding current of the VM, respectively. The state variable $x$ denotes the normalized relative conductivity between two competing conduction channels, ranging from 0 to 1. Specifically, $x = 0$ corresponds to a purely Schottky-dominated conduction process, whereas $x = 1$ indicates a purely tunneling-dominated process. The parameter $\alpha$ denotes the Schottky barrier height, while $\gamma$ characterizes the tunneling barrier height. The depletion width in the Schottky region is represented by $\beta$, and $\delta$ refers to the effective tunneling distance in the conductive path. The coefficient $\lambda$ modulates the relative weight of the two conduction mechanisms as a function of the applied voltage. The diffusion constant is denoted by $\tau$, and $\varepsilon$ quantifies the retention capability of the conductive filament. The material-related coefficients $\sigma$ and $\theta$ are linked to $\varepsilon$ and $\tau$, respectively. Moreover, $\eta_1$ and $\eta_2$ describe interfacial effects under positive and negative biases. All parameters are positive and depend solely on the intrinsic physical properties of the device materials, independent of the state variable $x$. Finally, the function $f(x)$ acts as a window function that constrains the evolution of the state variable within physically meaningful bounds. The detailed parameter values used in this work are listed in Table 1.

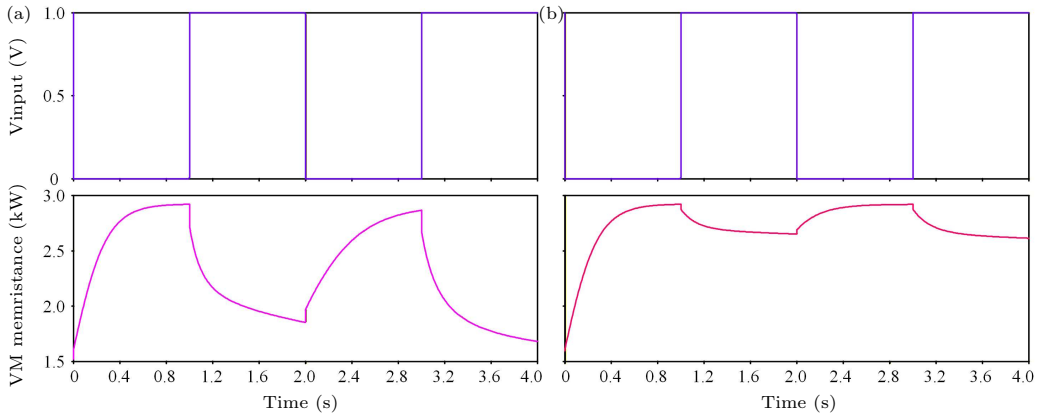



**Fig. 1.** Memristance responses of two VMs ) under a 1.0 V square-wave input. (a) VM1 with a 5 kΩ series resistor. (b) VM2 with a 1 kΩ series resistor.

**Table 1.** Parameter settings of the VM model.

| Parameters | $\alpha$ | $\beta$ | $\gamma$ | $\delta$ | $\lambda$ |
|---|---|---|---|---|---|
| Settings | $3\times10^{-4}$ | 0.2 | $1\times10^{-3}$ | 1 | 0.05 |
| Parameters | $\sigma$ | $\theta$ | $\eta_1$ | $\eta_2$ | |
| Settings | $1\times10^{-4}$ | 0.01 | 4 | 2 | |

A periodic square-wave voltage signal is applied to the VM, as illustrated in Fig. 1. During each voltage pulse, the memristance of the device decreases rapidly, reflecting its immediate response to external stimulation. Once the pulse is removed, the memristance gradually returns to its initial state, thereby reproducing the transient forgetting behavior characteristic of biological synapses. Two circuit configurations are evaluated, where the same VM is connected in series with resistors of 5 kΩ and 1 kΩ, respectively. The results show that a smaller series resistance leads to a lower effective memristance under stimulation and a slower relaxation process after the stimulus is withdrawn. In other words, reducing the series resistance decreases the VM's memristance and increases the subsequent input voltage applied to the next circuit stage, and vice versa. The detailed structure and functional role of the VM within the overall circuit framework will be further discussed in the subsequent circuit design section.

### 2.2. Non-volatile memristive model

In contrast to the VM, the non-volatile memristor (NVM) is capable of retaining its conductance state even after the removal of the external stimuli. This property enables the NVM to emulate the long-term memory functions of the brain and to mimic the modulation of synaptic weights observed in biological neurons. In this work, commercially available self-regulating channel memristors from Knowm Inc. (Santa Fe, NM, USA) are employed. The resistance variation of the device arises from the migration of $Ag^+$ ions within the active layer. To describe its behavior, the adaptive voltage threshold memristor (AVTM) model[7] is adopted, which can be expressed as follows:

$$u(t) = \left[R_{\rm off} - k(t)\left(R_{\rm off} - R_{\rm on}\right)\right] i(t), \tag{2}$$

where $R_{\rm on}$ and $R_{\rm off}$ correspond to the lower and upper bounds of the device memristance, respectively. The internal state variable $k(t)$ represents the normalized thickness of the conductive region, and its temporal evolution follows:

$$\frac{{\rm d}k(t)}{{\rm d}t} = \begin{cases} a_1\left[h(u(t)) + b_1\right] i(t) f(k(t)), & u(t) \geq 0, \\ a_2\left[h(u(t)) + b_2\right] i(t) f(k(t)), & u(t) < 0, \end{cases} \tag{3}$$

where $h(u(t))$ and $f(k(t))$ denote the voltage threshold function and the window function, respectively. The derivatives of $h(u(t))$ and $f(k(t))$ are as follows:

$$h(u(t)) = \begin{cases} \dfrac{u(t)}{u_{\rm on}}^{k_1}, & u(t) \geq 0, \\ \dfrac{u(t)}{u_{\rm off}}^{k_2}, & u(t) < 0, \end{cases} \tag{4}$$

$$f(k(t)) = \begin{cases} (1-k(t))^{p_1}, & i(t) \geq 0, \\ (k(t))^{p_2}, & i(t) < 0, \end{cases} \tag{5}$$

where $u_{\rm on}$ and $u_{\rm off}$ represent the positive and negative switching thresholds, respectively. The parameters $a$, $b$, $k$, and $p$ are model constants. In this work, the specific values are chosen as $R_{\rm off} = 600\ \Omega$, $R_{\rm on} = 175\ \Omega$, $a_1 = 7$, $a_2 = 95$, $b_1 = 0$, $b_2 = 0.005$, $p_1 = 3$, $p_2 = 8$, $k_1 = 2$, $k_2 = 5$, $u_{\rm on} = 0.1$ V, and $u_{\rm off} = -0.1$ V. When the applied voltage exceeds $u_{\rm on}$, the memristance decreases, whereas when the voltage falls below $u_{\rm off}$, the memristance increases, as demonstrated in the simulation results in Fig. 2.

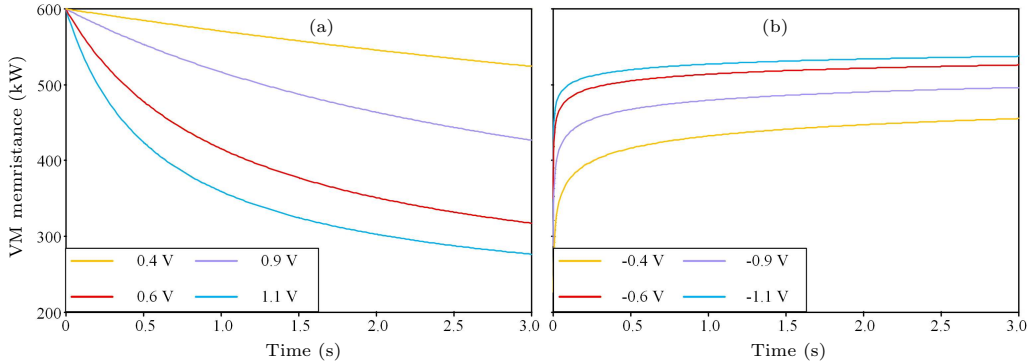



**Fig. 2.** Memristance curves of the NVM under various voltage inputs: (a) Memristance curves under positive voltages. (b) Memristance curves under negative voltages.

## 3. Behavioral modes under different stimulus conditions

During flight, as shown in Fig. 3, bats generate ultrasonic waves in their larynx, which are emitted through the mouth into the environment. When these ultrasonic pulses encounter insects or obstacles, the reflected echoes are received by the ears of the bat. By analyzing the time delay between sound emission and echo reception, the bat determines the position

and distance of the target. This biological mechanism,[43,44] known as echolocation, enables bats to navigate and hunt in complete darkness.

In this work, the echolocation mechanism is adopted as the bionic foundation for circuit design. The input signal of the circuit represents the external echo stimulus, whose intensity is inversely proportional to the distance between the bat and the target – the closer the target, the stronger the stimulus; the farther the target, the weaker the stimulus. This signal is applied to the stimulus module, providing the sensory input for subsequent decision-making processes.

This behavioral process can be categorized into three typical conditions, corresponding to three functional modes of the proposed memristive circuit framework.

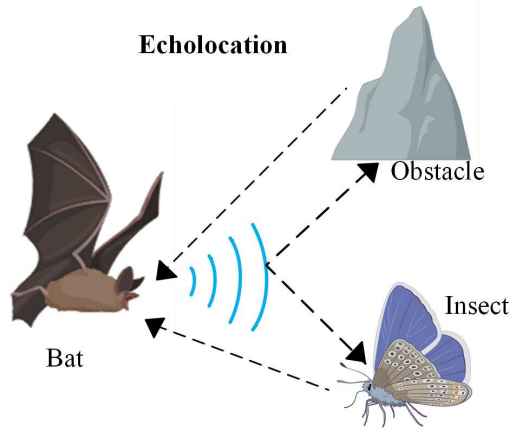



**Fig. 3.** Schematic illustration of the echolocation mechanism in a bat.

**(a) Strong stimulus condition** Under strong external echo stimulation, spatial information is accurately perceived, and immediate movement adjustment is achieved. As illustrated in Fig. 4(a), the echo signal corresponds to a high input voltage applied to the Stimulus (S) module. The signal is directly forwarded to the Action (A) module, producing a clear and immediate motor response. In this mode, the system behavior is dominated by the sensory input, resulting in fast and accurate directional control.

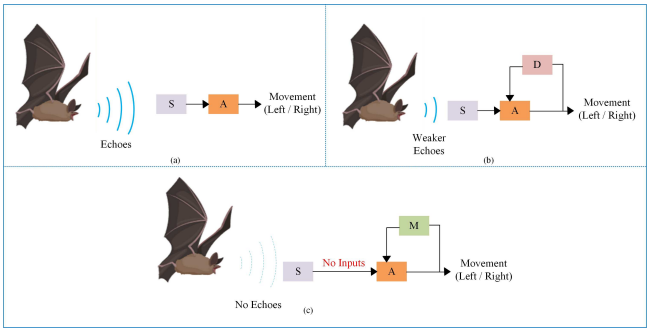



**Fig. 4.** Behavioral process and corresponding circuit framework under different stimulus conditions: (a) strong stimulus condition, (b) weak stimulus condition, and (c) no stimulus condition.

**(b) Weak stimulus condition** When the echo intensity decreases, sensory perception becomes less reliable. To ensure robust behavioral output, the Decision-making (D) module is activated to support the Action (A) module. As shown in Fig. 4(b), this mechanism is realized through an auxiliary voltage pathway that dynamically adjusts the decision threshold of the A module. Through internal modulation, stable movement decisions are maintained even under weak sensory conditions.

**(c) No stimulus condition** When no echo is received, external sensory information is unavailable. In this case, the Memory (M) module, as depicted in Fig. 4(c), becomes dominant and generates an internal bias voltage to sustain the output of the A module. This internally generated signal reflects previously stored spatial information, enabling the system to preserve its movement direction in the absence of input. In the proposed memristive circuit, this memory function is implemented using NVMs, whose resistance states encode spatial information and provide a stable bias for decision maintenance.

## 4. Circuit model design

### 4.1. Stimulus module and action module

The Stimulus (S) module, shown in Fig. 5, processes the external input $V_{\text{stimuli_R}}$ and converts it into an effective driving signal for the subsequent Action (A) module. The circuit integrates voltage filtering, logic-based reset, and signal summation mechanisms to ensure selective response and automatic recovery.

First, the external stimulus $V_{\text{stimuli_R}}$ is passed through an absolute-value rectifier (ABS), where negative components are converted into a positive amplitude

$$V_{\text{ABS}} = |V_{\text{stimuli_R}}|.$$

This operation mimics the preprocessing of auditory echoes in biological systems, ensuring that the subsequent circuitry responds to stimulus intensity regardless of polarity. The filtered signal is then processed by the comparator (COMP), which consists of a PMOS–NMOS pair functioning as a voltage threshold detector. In this circuit, the comparator employs two explicit threshold references: $T_1 = -2$ V and $T_2 = 2.5$ V. Only when the input voltage exceeds the defined threshold of approximately $V_{\text{th}} = 0.2$ V does the comparator conduct, allowing valid stimuli to propagate to the next stage. This behavior can be mathematically described as

$$V_{\text{Filtered_R}} = \begin{cases} 1, & V_{\text{ABS}} > V_{\text{th}}, \\ 0, & V_{\text{ABS}} \le V_{\text{th}}. \end{cases} \tag{6}$$

Next, the output from the filtering stage is combined with the reset node $V_{\text{re}} = 1$ V through a NOR gate, producing an inverted logic voltage that enables the reset function. When

the input disappears, the NOR gate outputs $V_{U1} = 1$ V, which is then amplified and inverted by operational amplifier OP1 as

$$V_{OP1} = -\frac{200}{1000} V_{U1}.$$

This negative feedback restores the baseline potential of the system and ensures that the S module automatically resets when no input is present. Finally, the outputs of the rectifier and the inverting amplifier are summed through the adder node `SUM1`, and the resulting voltage drives the memristor M1, expressed as

$$V_{M1} = V_{ABS} + V_{OP1}. \tag{7}$$

The Action (A) module, as illustrated in Fig. 5, receives the processed voltage from the memristor M1 and converts it into a corresponding output voltage $V_{Action_R}$, representing the behavioral response to the external stimulus. The input voltage $V_{M1}$ from the S module is first amplified by operational amplifiers OP2 and OP3. The output voltage $V_{OP3}$ is then compared with a reference threshold $V_{th} = 0.2$ V by transistor T3, which functions as a voltage-controlled comparator. The conduction state of T3 determines whether the system outputs a high or low behavioral voltage:

$$V_{T3} = \begin{cases} -1\text{ V}, & V_{OP3} > V_{th}, \\ 0\text{ V}, & V_{OP3} \le V_{th}. \end{cases} \tag{8}$$

When $V_{OP3} > 0.2$ V, the transistor turns on and the circuit generates a positive response signal. Conversely, when the input voltage falls below the threshold, the transistor remains off and no movement output is produced.

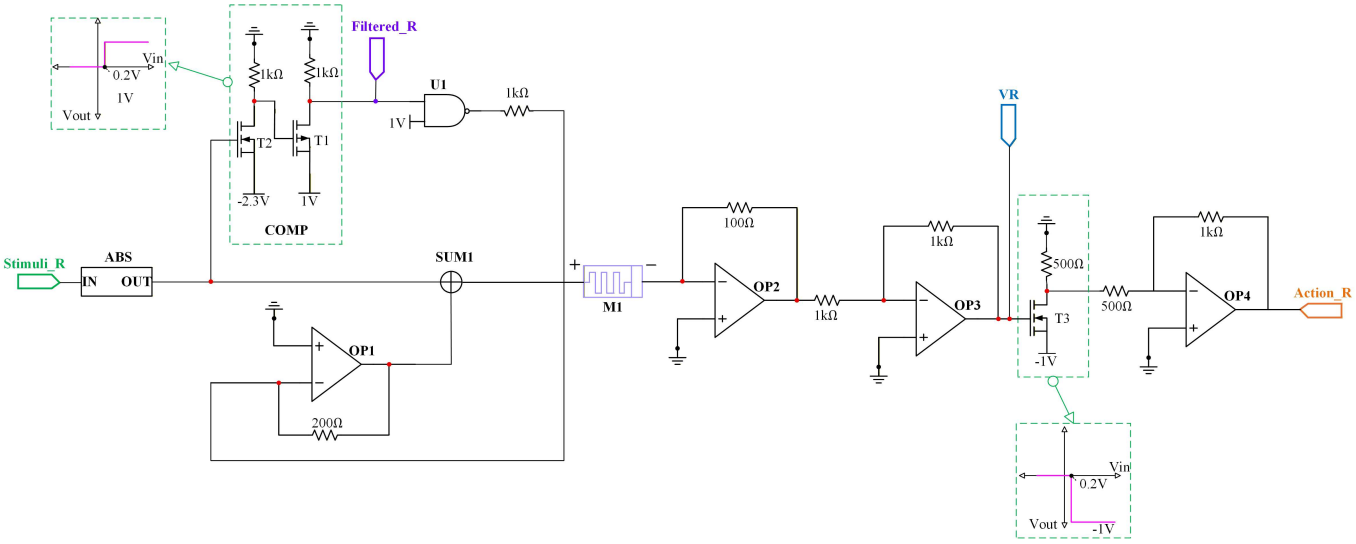



**Fig. 5.** Circuit schematic of the stimulus and action modules.

### 4.2. Decision-making module

The Decision-making (D) module is primarily engaged when the external stimulus is weak, assisting the system in determining the correct behavioral direction. Its main functions include pathway comparison, voltage integration, and reset regulation, as illustrated in Fig. 6. When the stimulus is strong, the S and A pathways dominate, and the D module remains inactive. Two AND gates (U2, U3) first detect which left or right pathway has produced an action response. The corresponding AND gate outputs a high voltage

$$\begin{cases} V_{U2} = V_{Filtered_L} \cdot V_{Action_L}, \\ V_{U3} = V_{Filtered_R} \cdot V_{Action_R}. \end{cases} \tag{9}$$

The outputs of U2 and U3 are then merged through the OR gate U4 to generate a combined decision voltage

$$V_{U4} = V_{U2} + V_{U3}. \tag{10}$$

This combined voltage drives the VM, whose internal memristance represents the transient decision state. Unlike NVMs, the VM exhibits self-recovery behavior once the input signal disappears, meaning that its memristance gradually returns to the initial state without external control. This feature allows the circuit to operate primarily under weak stimulus conditions and to automatically reset during the inter-trial resting period, preventing decision bias accumulation. In this work, the VM is intentionally selected for its short-term memory characteristics: it can temporarily store decision-related information when the stimulus is present, yet naturally erase this memory when the stimulus is removed. This volatility-based self-resetting mechanism eliminates the need for additional reset circuitry and ensures that each decision cycle begins from a neutral, unbiased state, which is essential for reliable behavioral computation in repeated trials.

The memristor output voltage $V_{M2}$ is then successively

amplified by two operational amplifiers and subsequently fed into the comparator OP7, yielding the differential decision potential

$$V_{\mathrm{OP7}} = \begin{cases} 2\ \mathrm{V}, & V_{\mathrm{M2}} > 0.1\ \mathrm{V}, \\ -2\ \mathrm{V}, & V_{\mathrm{M2}} \leq 0.1\ \mathrm{V}. \end{cases} \tag{11}$$

This output distinguishes whether the previous behavioral choice is correct or incorrect. When $V_{\mathrm{SUM2}} < -0.1$ V, T3 conducts, re-stabilizing the circuit toward its resting level

$$V_{\mathrm{T3}} = \begin{cases} 1\ \mathrm{V}, & V_{\mathrm{SUM2}} < 0.1\ \mathrm{V}, \\ 0\ \mathrm{V}, & V_{\mathrm{SUM2}} \geq -0.1\ \mathrm{V}. \end{cases} \tag{12}$$

Finally, the reset-adjusted decision potential is sent to two logic gates (U6, U7) for AND operations with the filtered left and right signals, respectively,

$$\begin{cases} V_{\mathrm{Choice_L}} = V_{\mathrm{Filtered_L}} \cdot V_{\mathrm{T3}}, \\ V_{\mathrm{Choice_R}} = V_{\mathrm{Filtered_R}} \cdot V_{\mathrm{T3}}. \end{cases} \tag{13}$$

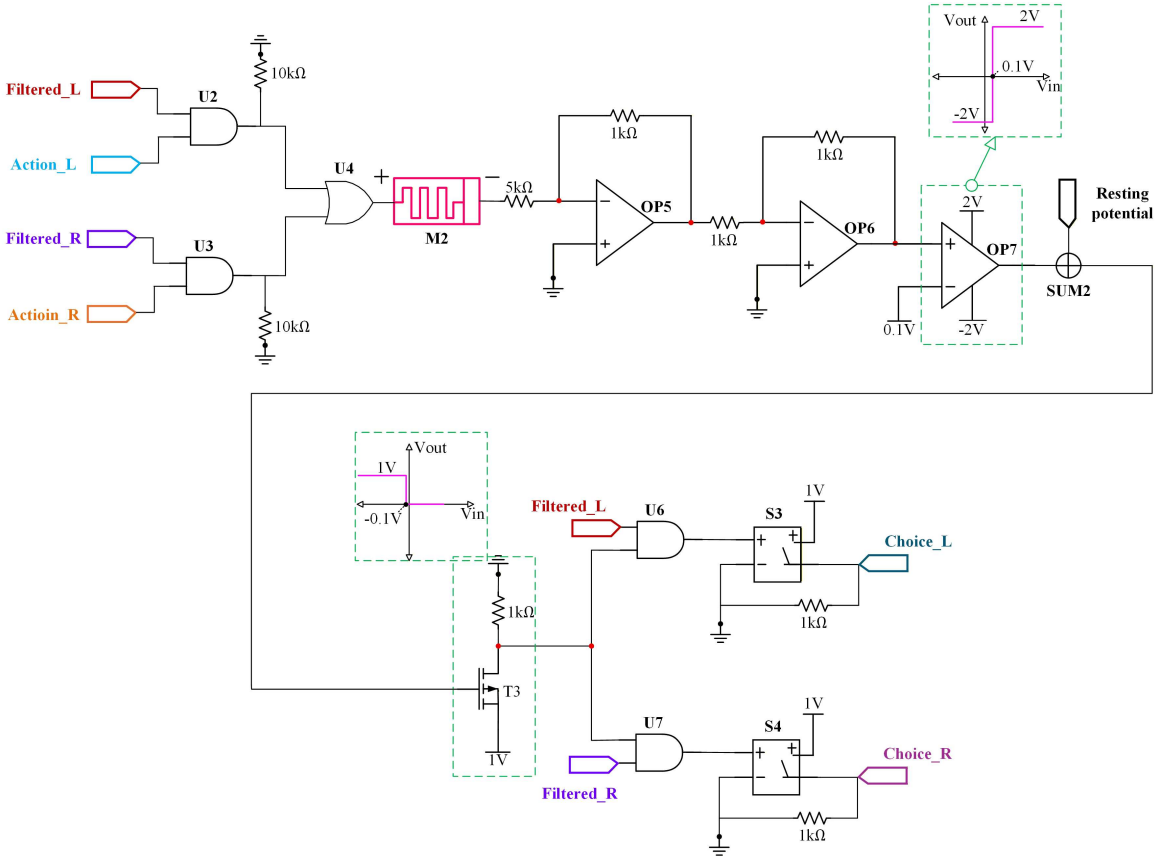



**Fig. 6.** Circuit schematic of the decision-making module.

### 4.3. Memory module

The Memory (M) module is primarily engaged when external stimuli disappear, maintaining behavioral continuity based on previously stored information. Biologically, this process corresponds to the short-term persistence of neuronal activity after sensory input vanishes, enabling animals to complete motion sequences from memory. As shown in Fig. 7, the proposed circuit emulates this process by extracting and retaining the action potentials ($V_{\mathrm{L}}$, $V_{\mathrm{R}}$) generated in the A module during the previous trial. In PSPICE, this is implemented using ABM elements, which employ Laplace-based transfer functions to establish a mathematical relationship between input and output signals. This configuration allows the ABM modules to temporarily store or delay voltage information, effectively reproducing the memory retention observed in biological systems. In the proposed model, each ABM unit extracts the voltage value from the previous trial period and applies it to the decision-making process of the current cycle. The specific voltage values are calculated as

$$\begin{cases} V_{\mathrm{T-1_L}} = V_{\mathrm{L}}(t-T), \\ V_{\mathrm{T-1_R}} = V_{\mathrm{R}}(t-T). \end{cases} \tag{14}$$

The delayed voltages $V_{\mathrm{T-1_L}}$ and $V_{\mathrm{T-1_R}}$ are first processed by operational amplifiers OP8 and OP9, which act as subtraction units to calculate the voltage difference between the two memory traces. Whichever output yields a positive result corresponds to the dominant direction in the previous trial,

and a high-level voltage $V_{\text{high}} = 1$ V is generated at that side to indicate the preferred movement pathway. Meanwhile, the filtered signals $V_{\text{Filtered_L}}$ and $V_{\text{Filtered_R}}$ are processed through a NOT–OR logic element, where the output is combined with the reset potential. This configuration provides the same recovery mechanism as in the D module, ensuring that the circuit can automatically return to its resting state between trials.

In addition, ABM3 and ABM4 function as decision comparators that determine the sign of the subtraction results. Each ABM block implements a voltage-evaluation rule of the form

$$V_{\text{out}} = \begin{cases} 0, & V_{\text{input}} > 0, \\ -1\ \text{V}, & V_{\text{input}} \le 0, \end{cases} \tag{15}$$

which corresponds to the conditional expression used in the simulation model. In this manner, ABM3 processes the left delayed trace $V_{\text{T}-1_\text{L}}$, while ABM4 evaluates the right delayed trace $V_{\text{T}-1_\text{R}}$. The outputs of ABM3 and ABM4 encode whether the respective directional memory exhibits a positive or negative dominance, enabling the M module to distinguish the stronger bias from the previous trial.

Finally, the resulting reset potential is summed with the memory voltages obtained from ABM3 and ABM4, producing the final output of the M module and establishing a bias voltage that guides the decision-making process in the subsequent trial.

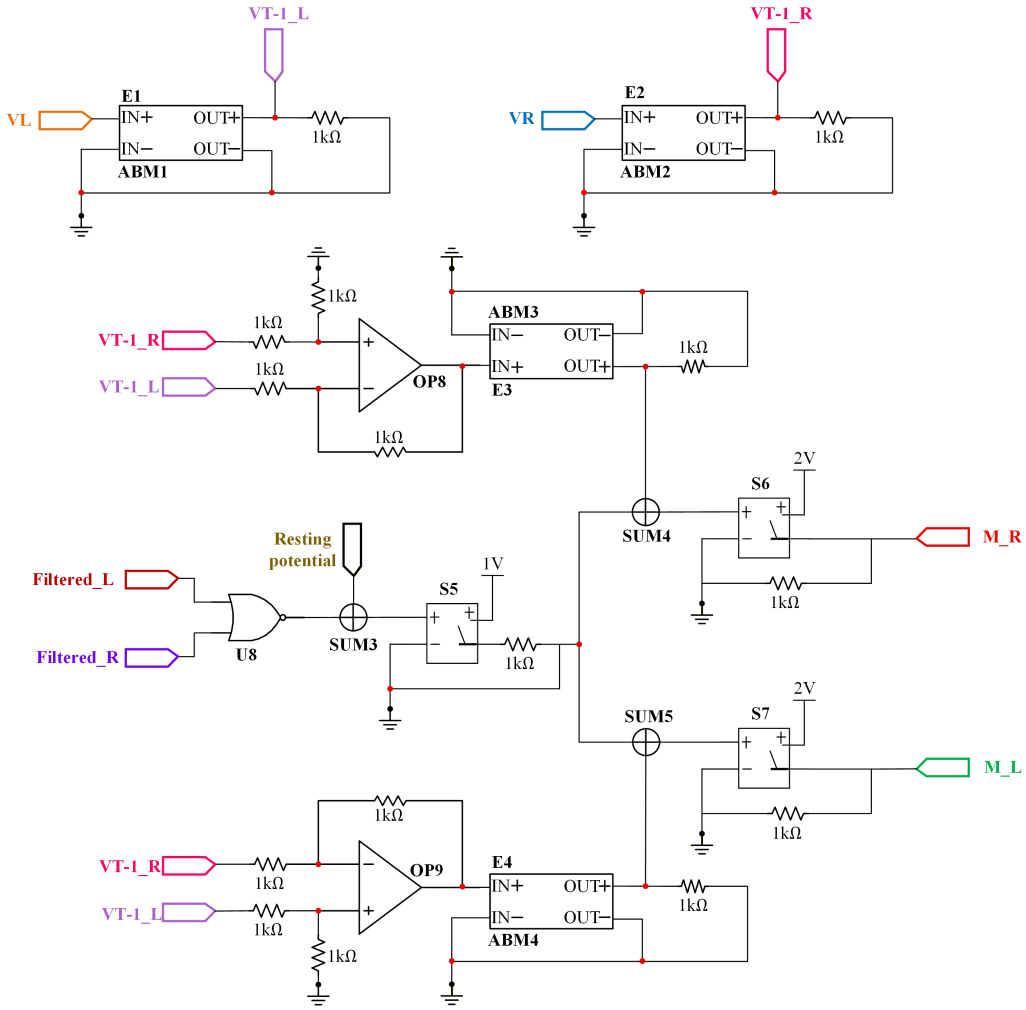



**Fig. 7.** Circuit schematic of the Memory module.

### 4.4. Complete circuit

As shown in Fig. 8, the proposed system integrates the S, A, D, and M modules into a unified architecture. Each module corresponds to a distinct stage of the biological decision-making process, jointly forming a continuous functional pathway from external perception to behavioral output. The S module filters and rectifies the external stimuli to produce effective driving voltages; the A module converts these inputs into directional motor responses; the D module provides compensatory regulation under weak stimulus conditions to ensure stable decision performance; and the M module preserves behavioral continuity by generating memory-based bias voltages when external inputs vanish.

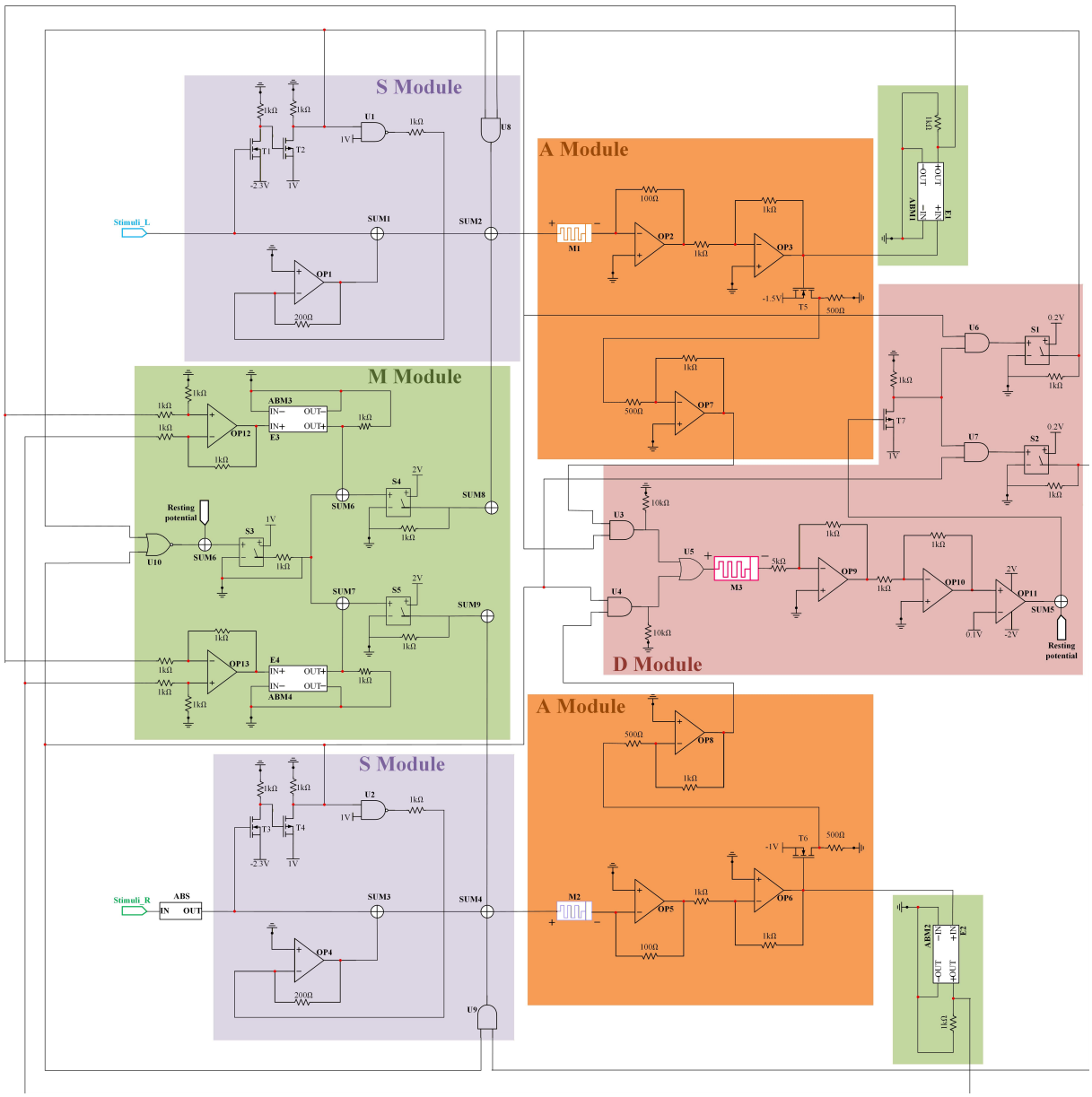



**Fig. 8.** Complete circuit structure for S module, A module, D module and M module.

In addition, the system incorporates several explicitly defined threshold references to ensure reliable state transitions across modules. Specifically, the comparator thresholds are set to $T_1 = -2$ V, $T_2 = 2.5$ V, $T_3 = -2$ V, $T_4 = 2.5$ V, $T_5 = 1.7$ V, $T_6 = 1.2$ V, and $T_7 = -2$ V, each governing distinct switching operations within the S, A, D, and M modules.

## 5. Simulation

The proposed circuit is simulated in PSPICE to evaluate its functional behavior under different stimulus conditions. The simulations are divided into three scenarios, corresponding to strong, weak, and no stimulus inputs. Each simulation sequence consists of 15 consecutive trials, in which left or right stimuli are randomly applied, and each trial lasts 1.5 s.

### 5.1. Simulation under strong stimulus condition

Under strong stimulus conditions, the behavioral response of the system is primarily driven by external sensory inputs. As shown in Fig. 9, distinct voltage pulses are applied to the left and right channels to represent the sensory stimuli. When a strong stimulus is presented, the corresponding memristors (M1 and M2) exhibit a rapid decrease in memristance, indicating an enhanced synaptic potentiation process. This variation in memristance enables stronger voltage transmission toward the A module, producing a clear output signal that corresponds to the external input.

The simulation results reveal that accurate movement responses are produced in response to the applied stimuli. A precise one-to-one correspondence between stimulus and action is maintained in each trial, confirming that fast and re-

liable decision-making behavior is effectively reproduced under strong excitation. Under this condition, both the D and M modules remain inactive, and the overall behavioral process is governed by direct sensory pathways.

### 5.2. Simulation under weak stimulus condition

Under weak stimulus conditions, the circuit activates the internal decision-regulation mechanism to compensate for insufficient sensory input. As shown in Fig. 10, when the external stimulus voltage applied to the left or right channel decreases, the response of the primary sensory pathway becomes less reliable. In this situation, the D module is engaged to assist the behavioral output. The transient memristor M3, characterized by its volatile memory property, exhibits a temporary decrease in resistance during stimulus presentation, followed by a gradual recovery once the stimulus vanishes.

The simulation results show that when the stimulus is weak, the auxiliary voltage generated by the D module effectively enhances the action potential in the correct channel, allowing the system to make the proper choice even under degraded sensory conditions. This demonstrates that the proposed circuit can achieve reliable behavioral decisions through internal adjustment when sensory cues are weak or ambiguous.

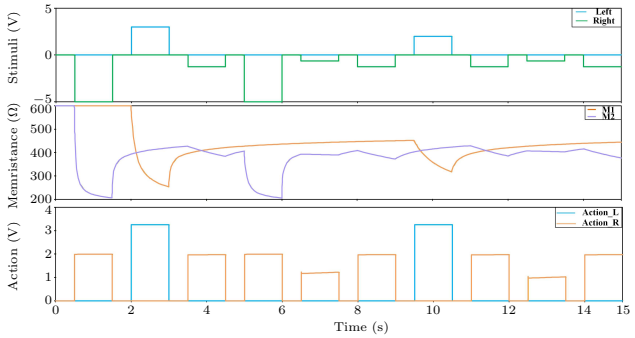



**Fig. 9.** Simulation results under strong stimulus condition.

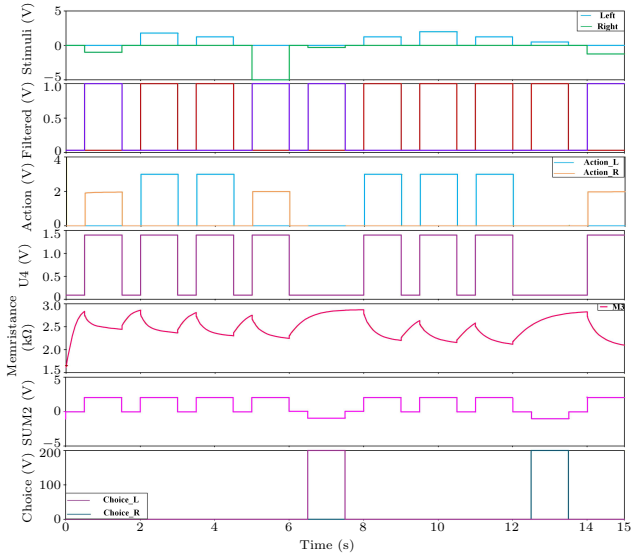



**Fig. 10.** Simulation results under weak stimulus condition.

### 5.3. Simulation under no stimulus condition

Under no-stimulus conditions, the circuit demonstrates memory-dependent decision-making behavior in the absence of external sensory input. As shown in Fig. 11, when the external stimulus signal disappears, both sensory channels cease to provide effective input. At this stage, the system activates the M module to sustain the behavioral response through internally stored information. The ABM units extract and retain the action voltages from the previous trial, denoted as $V_{\mathrm{T-1_L}}$ and $V_{\mathrm{T-1_R}}$, and reintroduce them into the current decision process. By comparing these voltages, the circuit determines which channel exhibited stronger activation in the previous cycle and generates a corresponding bias voltage to guide the present choice.

The simulation results reveal that even without external stimulation, the system successfully maintains correct behavioral responses consistent with previous experience. The memristor states remain stable during the no-input interval, reflecting the persistence of long-term memory traces. Once the subsequent stimulus reappears, the circuit rapidly resumes normal sensory-driven behavior without delay. This result demonstrates that the proposed model effectively emulates memory-guided decision-making, allowing stable operation even in the absence of sensory cues.

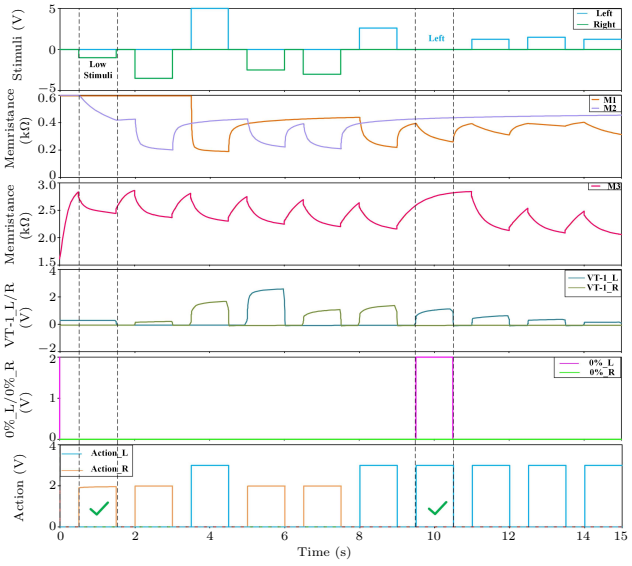



**Fig. 11.** Simulation results under no stimulus condition.

**Table 2.** Comparisons between the proposed work and other similar works.

| Work | Decision bias | Weak stimulus handling | VM+NVM Synapse |
|---|---|---|---|
| Ref. [45] | X | X | X |
| Ref. [46] | X | X | X |
| Ref. [47] | X | X | X |
| Ref. [48] | X | X | X |
| This work | ✓ | ✓ | ✓ |

Compared with previous studies shown in Table 2, the proposed circuit exhibits a higher level of functional integra-

tion by supporting decision bias, weak-stimulus compensation, and a "VM+NVM" synaptic structure within a unified framework. Unlike prior designs that focus on only one or two aspects, the present work offers a comprehensive behavioral decision mechanism that more closely reflects biological processing and ensures stable operation across varying stimulus conditions.

## 6. Conclusion

In this work, an echolocation-inspired memristive behavioral decision circuit is proposed, integrating stimulus sensing, action generation, decision-making, and memory modules into a unified architecture. PSPICE simulations demonstrate that the system produces a clear stimulus-to-response mapping under strong sensory inputs, while weak or ambiguous stimuli are compensated through internal decision regulation, ensuring stable and accurate behavioral outputs. Furthermore, when no external input is available, the memory module preserves previously formed associations, enabling the circuit to generate consistent, memory-guided decisions. These results show that the proposed design effectively reproduces key characteristics of biological behavioral control and provides a circuit solution for implementing biologically inspired decision-making mechanisms.

## Acknowledgments

This project was supported by the National Natural Science Foundation of China (Grant No. 62571079), the Technological Innovation Projects in the Field of Artificial Intelligence in Liaoning Province (Grant No. 2023JH26/10300011), the Basic Scientific Research Projects of the Department of Education of Liaoning Province (Grant No. LJ212410152049), and the Liaoning Provincial Science and Technology Plan Joint Project (Grant No. 2024-MSLH-033).

## References

[1] Combrisson E, Basanisi R, Neri M, Auzias G, Petri G, Marinazzo D, Panzeri S and Brovelli A 2025 *Nat. Commun.* **16** 7179
[2] Angelaki D, Benson B, Benson J, Birman D, Bonacchi N, Bougrova K, Bruijns S A, Carandini M and Catarino J A 2025 *Nature* **645** 177
[3] Montagrin A, Croote D E, Preti M G, Lerman L, Baxter M G and Schiller D 2024 *Nat. Commun.* **15** 4815
[4] Li C, Li Y, Yu W, Moroz I and Volos C 2025 *Nonlinear Dyn.* **113** 3857
[5] Yu F, Kong X, Yao W, Zhang J, Cai S, Lin H and Jin J 2024 *Chaos Solitons Fract.* **179** 114440
[6] Chen L, Li C, Huang T, Chen Y, Wen S and Qi J 2013 *Phys. Lett. A* **377** 3260
[7] Guo M, Zhu Y, Liu R, Zhao K and Dou G 2022 *Neurocomputing* **472** 12
[8] Gao S, Iu H C, Erkan U, Simsek C, Toktas A, Cao Y, Wu R, Mou J, Li Q and Wang C 2025 *IEEE Trans. Circuits Syst. Video Technol.* **35** 7706
[9] Gao S, Zhang Z, Li Q, Ding S, Iu H H C, Cao Y, Xu X, Wang C and Mou J 2025 *IEEE Trans. Dependable Secure Comput.* **22** 8011
[10] Huang B, Liu Y, Jiang Y L and Wang J 2024 *Neural Netw.* **169** 83
[11] Hasani R, Lechner M, Amini A, Liebenwein L, Ray A, Tschaikowski M, Teschl G and Rus D 2022 *Nat. Mach. Intell.* **4** 992
[12] Zheng H, Zheng Z, Hu R, Xiao B, Wu Y, Yu F, Liu X, Li G and Deng L 2024 *Nat. Commun.* **15** 277
[13] Chen X, Sun K, Wang H, Liu J and Yao Z 2025 *Chaos Solitons Fract.* **201** 117189
[14] Wang H, Chen H, Sun K, Zhu W and Yao Z 2025 *Nonlinear Dyn.* **113** 10365
[15] Mou J, Zhang Z, Banerjee S and Zhang Y 2024 *IEEE Internet Things J.* **11** 33565
[16] Han Z, Cao Y, Banerjee S and Mou J 2025 *Chin. Phys. B* **34** 030503
[17] Lei Z, Guo Y, Ma J and Wang C 2025 *Chaos Solitons Fract.* **201** 117384
[18] Zhang Z, Cao Y, Zhou N, Xu X and Mou J 2025 *Appl. Intell.* **55** 61
[19] Tian X, Wu F and Ma J 2025 *Chaos Solitons Fract.* **199** 116828
[20] Yu F, Su D, He S, Wu Y, Zhang S and Yin H 2025 *Chin. Phys. B* **34** 050502
[21] Yang F, Song X and Xu Y 2025 *Chaos Solitons Fract.* **199** 116740
[22] Yang F, Song X and Yu Z 2025 *Nonlinear Dyn.* **113** 7213
[23] Chua L 2003 *IEEE Trans. Circuit Theory* **18** 507
[24] Zhang Y and Zeng Z 2023 *IEEE Trans. Cogn. Dev. Syst.* **16** 1707
[25] Song Y, Gao S and Xu X Y 2025 *Int. J. Bifurcation Chaos* **36** 2650019
[26] Sun J, Zhai Y, Liu P and Wang Y 2024 *IEEE Trans. Neural Netw. Learn. Syst.* **36** 3618
[27] Shi F, Cao Y, Xu X, Banerjee S and Mou J 2026 *Chaos Solitons Fract.* **202** 117435
[28] Li H, Jiang C and Hua Q 2025 *Sensors* **25** 1533
[29] Nelapati R P 2025 *Eng. Res. Express* **7** 015363
[30] Lu J, Ran H, Xie D, Zhou G and Hu X 2025 *Chin. Phys. B* **34** 018703
[31] Li X, Jiang J, Liu G, Zhou B and Zhao E 2024 *J. Mater. Sci. Mater. Electron.* **35** 1608
[32] Wang H, Yang Y, Fu Q and Wang D 2025 *Int. J. Circuit Theory Appl.* **53** 708
[33] Xiong D, Wang X, Jiang Y, Yang C, Jiang M, Lai J and Zeng Z 2025 *IEEE Trans. Cogn. Dev. Syst.* **17** 1186
[34] Yang C, Wang X, Chen Z, Zhang S and Zeng Z 2022 *IEEE Trans. Biomed. Circuits Syst.* **16** 926
[35] Wan Q, Liu J, Liu T, Sun K and Qin P 2024 *Neural Netw.* **174** 106268
[36] Selesnick S 2024 *J. Comput. Neurosci.* **52** 223
[37] Chen H, Hong Q, Liu W, Wang Z and Zhang J 2022 *IEEE Trans. Cogn. Dev. Syst.* **15** 1289
[38] Sun J, Chen Y, Wang Z and Wang Y 2025 *IEEE Trans. Ind. Inform.* **21** 9909
[39] Zhang M, Wang C, Sun Y and Li T 2024 *Nonlinear Dyn.* **112** 4841
[40] Wang Y C, Zhao Y, Sun J, Wang Y and Wang Y F 2024 *Eur. Phys. J. Plus* **139** 320
[41] Yu Z, Zhu K, Wang Y and Yang F 2025 *Chaos Solitons Fract.* **194** 116233
[42] Kim N, Nirmal K A, Lee H J and Kim T G 2025 *Small* **21** e06631
[43] Beetz M J, Hechavarría J C and Kössl M 2016 *Sci. Rep.* **6** 35991
[44] Beetz M J and Hechavarría J C 2022 *Front. Neural Circuits* **16** 899370
[45] Tang Z, Wang X, Yang C, Chen Z and Zeng Z 2024 *IEEE Trans. Biomed. Circuits Syst.* **18** 552
[46] Sun J, Yang J, Wang Y, Liu P and Sheng Y 2023 *IEEE Trans. Circuits Syst. I Regul. Pap.* **70** 2331
[47] Sun J, Wang Y, Liu P, Wen S and Wang Y F 2022 *IEEE Trans. Cybern.* **53** 3351
[48] Zhou H, Fei Z, Hong Q, Sun J, Du S, Li T and Zhang J 2022 *IEEE Trans. Cogn. Dev. Syst.* **15** 1196